SENSITIVITY STUDIES FOR *IN-SITU* AUTOMATED TAPE PLACEMENT OF THERMOPLASTIC COMPOSITES

Robert C. Costen
NASA Langley Research Center
Hampton, VA

Joseph M. Marchello
Old Dominion University
Norfolk, VA

ABSTRACT

This modeling effort seeks to improve the interlaminate bond strength of thermoplastic carbon composites produced by the *in-situ* automated tape placement (ATP) process. An existing high productivity model is extended to lower values of the Peclet number that correspond to the present operating conditions of the Langley ATP robot. (The Peclet number is the dimensionless ratio of inertial to diffusive heat transfer.) In sensitivity studies, all of the process and material parameters are individually varied. The model yields the corresponding variations in the effective bonding time (EBT) referred to the glass transition temperature. According to reptation theory, the interlaminate bond strength after wetting occurs is proportional to the one-fourth power of EBT. The model also computes the corresponding variations in the thermal input power (TIP) and the mass and volumetric process rates. Process studies show that a 10 percent increase in the consolidation length results in a 20 percent increase in EBT and a 5 percent increase in TIP. A surprising result is that a 10 K *decrease* in the tooling temperature results in a 25 percent increase in EBT and an 8 percent increase in TIP. Material studies show that a 10 K decrease in glass transition temperature results in an 8 percent increase in EBT and a 8 percent decrease in TIP. A 20 K increase in polymer degradation temperature results in a 23 percent increase in EBT with no change in TIP.

KEY WORDS: Modelling, Carbon Fibers, Thermoplastic Polymers, Composites, PEEK/C.

1. INTRODUCTION

Carbon fiber composites have greater strength and stiffness per unit mass than most materials used in aerospace applications. However, the fabrication of aircraft wings and fuselages from such composites is relatively expensive. *In-situ* automated tape placement (ATP) is a process

---

aimed at reducing this cost. Thermoplastic carbon composite tape -- typically of thickness $\tau = 1.27 \times 10^{-4}$ m and width $w = 0.0762$ m -- is laid down and thermally welded under pressure to a previous layer of ribbon to build up a laminated part.

The *in-situ* ATP process has been modeled extensively, as reported in references 1-10 However, a question that needs further attention is the following: What design changes in either the process or in the bulk properties of the composite would increase the interlaminate bond strength, decrease the thermal input power, or otherwise benefit the *in-situ* ATP process? To address this question, the authors will extend a thermal model given in reference 10 and perform sensitivity studies. The Peclet number Pe (dimensionless ratio of inertial to diffusive heat transfer) in the model will be reduced by two orders of magnitude so that it corresponds to the present operating conditions of the Langley ATP robot. The model determines the effective bonding time t_{eff} referred to the glass transition temperature T_g, the thermal input power Q_0, and the mass and volumetric process rates $\dot{M}$ and $\dot{V}$. According to reptation theory, as presented in reference 9, the interlaminar bond strength builds as $t_{eff}^{1/4}$ after wetting occurs until full strength is reached.

In the model, t_{eff}, Q_0, $\dot{M}$, and $\dot{V}$ are functions of the both the process variables and the bulk properties of the composite. The process variables include the tape width w and thickness τ, the laydown speed U, the consolidation length x_h, and the temperature of the tooling at infinity T_∞. The bulk properties of the composite include its density ρ, specific heat at constant pressure C_p, and longitudinal and transverse thermal conductivities K_{11} and K_{22}. These bulk properties can be modified by design to some extent. Hence, they are included in the sensitivity studies.

2. MODEL

The model uses an extended consolidation head of length x_h, as shown in Figure 1. Heat is applied at the nip $(x = 0, y = 0)$. The thermal input power per unit depth is given by $q_0 = Q_0 / w$. This head configuration is similar to that reported in reference 11; however, *all* consolidation heads, including hard rollers, have *finite* consolidation lengths because of the pliability of heated composites. The consolidation head and the supporting tool are thermally conducting. Far away from the nip, the tool and head are maintained at temperature T_∞. The conductivities of the tool and head are both taken equal to the average thermal conductivity of the composite substrate. As shown in reference 10, this assumption, together with the assumption that $Pe >> 1$, enables the temperature field $T(x,y)$ to be determined by the classical two-dimensional solution for a line thermal source in an infinite, moving, anisotropic conductor with the boundary condition that $T = T_\infty$ at infinity.

The thermal input power density q_0 is constrained so that the temperature on the weld interface $T(x,0)$ decreases passively to the glass transition temperature T_g at the downstream end of the consolidation head, where $x = x_h$. This constraint insures that the composite does not expand after consolidation pressure is released.

The classical solution is then nondimensionalized by introducing the following dimensionless (primed) variables:

$$x' \equiv \frac{x}{x_h} \tag{1a}$$

$$y' \equiv \left(\frac{K_{11}}{K_{22}}\right)^{1/2} \frac{y}{x_h} \tag{1b}$$

$$b \equiv \frac{\rho C_p U x_h}{2K_{11}} = \frac{Pe}{2} \tag{1c}$$

$$T' \equiv \frac{T(x,y) - T_\infty}{T_g - T_\infty} \tag{1d}$$

$$q_0' \equiv \frac{q_0}{2\pi (K_{11}K_{22})^{1/2} (T_g - T_\infty)} \tag{1e}$$

The classical solution for the dimensionless temperature T' is then given by (ref. 10)

$$T'(x',y') = \frac{\exp(bx') K_0 \left[b\left(x'^2 + y'^2\right)^{1/2} \right]}{\exp(b) K_0(b)} \tag{2a}$$

and that for the dimensionless thermal input power density q_0' by

$$q_0' = \frac{1}{\exp(b) K_0(b)} \tag{2b}$$

where K_0 is the hyperbolic Bessel function of zero order that is bounded at infinity. The thermal input power (in W) is given by

$$Q_0 = \frac{2\pi w (T_g - T_\infty)(K_{11}K_{22})^{1/2}}{\exp(b) K_0(b)} \tag{3a}$$

For $b \geq 10$, this result can be approximated by

$$Q_0 \approx 2w (T_g - T_\infty)(\pi \rho C_p K_{22} U x_h)^{1/2} \qquad (b \geq 10) \tag{3b}$$

3. PARAMETERIZATIONS

The solution (2a) for dimensionless temperature $T'(x',y')$ depends upon only one dimensionless parameter b. Isotherms in the substrate $(y' < 0)$ are plotted in Fig. 2 for $b = 10,\ 100$, and 1000. The isotherms for $y' > 0$ are mirror reflections of those shown. Thermal input occurs at $x' = y' = 0$. Pressure is applied by the consolidation head over the range $(0 \leq x' \leq 1)$. According to this figure, the model's use of passive cooling avoids the problem of temperature springback on the weld interface downstream of the consolidation head, as experienced by a model that uses active cooling (ref. 6).

Isotherm depth of penetration into substrate. The isotherms shown in Fig. 2 can be characterized by their width $\Delta x'(T',b)$ and depth of penetration into the substrate $y'_{\max}(T',b)$. The depth of penetration $y'_{\max}(T',b)$ is plotted in Fig. 3. High penetration is desirable because reheating previous layers under the consolidation head promotes bonding. Therefore, the increasingly rapid falloff of $y'_{\max}(T',b)$ as T' increases for $b<1000$ represents a loss of bonding efficiency. In reference 10, b was restricted to equal or exceed 1000. Here, new parameterizations allow b to be as small as 10. For $b\ge 10$, $y'_{\max}(T',b)$ is approximated by the parameterization

$$y'_{\max}(T',b)\approx \frac{.6065}{b^{1/2}T'}10^{\log\left(\frac{.6065}{b^{1/2}T'}\right)H_{m(b)}\left[\log\left(\frac{T'}{s(b)}\right)\right]} \qquad (b\ge 10;1\le T'\le 10) \quad (4a)$$

where

$$m(b)\equiv 1.808(b-8.829)^{-.027} \quad (4b)$$

$$s(b)\equiv 1.5761(b+.4805)^{.7821} \quad (4c)$$

$$H_\alpha(\beta)\equiv \frac{1}{2}\left[1+\tanh(\alpha\beta)\right] \quad (4d)$$

Here $H_\alpha(\beta)$ is the hyperbolic tangent representation for the unit step function, as discussed in reference 12, where the index α controls the rise steepness near $\beta=0$. The exact and parameterized curves for $y'_{\max}$ versus T' are shown for $b=10$, 100, and 1000 in Fig. 4.

Isotherm Width. Since the consolidation head applies pressure only on the interval $(0\le x'\le 1)$, any heating upstream of the nip does not contribute directly to bonding. Hence, the total isotherm width does not contribute to bonding. The part that does can be conservatively taken as the positive segment $\Delta x'_+(T',b)$ of the x' - axis that is enclosed by the T' -isotherm. This segment is plotted versus T' for various b in Fig 5. Again, the increasingly rapid falloff of $\Delta x'_+(T',b)$ as T' increases for $b<1000$ indicates a loss of bonding efficiency. For $b\ge 10$, these curves are approximated by the parameterization

$$\Delta x'_+(T',b)\approx \frac{10^{-[2+p(b)]\left(\log T'\right)H_{.19}\left[\log\left(\frac{T'}{r(b)}\right)\right]}}{T'^{[2+p(b)]}} \qquad (b\ge 10;1\le T'\le 10) \quad (5a)$$

where

$$p(b)\equiv 12.7528\left[1-H_{.7}(3+\log b)\right] \quad (5b)$$

$$r(b)\equiv 4.75b^{.5785} \quad (5c)$$

The exact and parameterized curves for $\Delta x'_+$ versus T' are shown for $b = 10$, 100, and 1000 in Fig. 6.

4. TEMPERATURE VERSUS TIME

The accumulated time interval $\Delta t(T)$ that the temperature at a material point on the weld interface is equal to or greater than T while pressure is being applied can be determined as follows: During the initial heating, the temperature at the point equals or exceeds T while under pressure for a period $\Delta x_+(T)/U$. As additional plies are added, the point can be reheated to temperature T or above. The total number of such heatings, including the initial heating, is given conservatively by $y_{\max}(T)/\tau$, where τ is the ply thickness. Each time the point is reheated, the period when the temperature equals or exceeds T becomes shorter. This shortening can be accounted for by a factor $\pi/4$, which is the area ratio for an ellipse and its circumscribed rectangle. The resultant formula for $\Delta t(T)$ is given by

$$\Delta t(T) = \frac{\pi}{4}\frac{\Delta x_+(T)}{U}\frac{y_{\max}(T)}{\tau} \tag{6}$$

Test computations with a wide range of isotherms and values for b confirm that (6) is a moderately conservative formula. It can be expressed in terms of the dimensionless variables by using (1), as follows

$$\Delta t(T') = \frac{\pi}{4}\left(\frac{K_{22}}{K_{11}}\right)^{1/2}\frac{x_h^{\,2}}{U\tau}\Delta x'_+\left(T'\right)y'_{\max}\left(T'\right) \tag{7}$$

Substitution of the parameterizations (4) and (5) then yields

$$\Delta t(T') \approx \frac{.6737}{(T')^3\tau}\left(\frac{K_{22}}{\rho C_p}\right)^{1/2}\left(\frac{x_h}{U}\right)^{3/2}E(T',b) \qquad \left(b \ge 10; 1 \le T' \le 10\right) \tag{8a}$$

where $E(T',b)$ is the bonding efficiency discussed in section 3. It is given by

$$E(T',b) \equiv \frac{10^{\left(\log\left(\frac{.6065}{b^{1/2}T'}\right)H_{m(b)}\left[\log\left(\frac{T'}{s(b)}\right)\right]-[2+p(b)]\left(\log T'\right)H_{19}\left[\log\left(\frac{T'}{r(b)}\right)\right]\right)}}{(T')^{p(b)}}$$

$$\left(b \ge 10; 1 \le T' \le 10\right) \tag{8b}$$

The bonding efficiency has the range $(0 \le E(T',b) \le 1)$ and a contour plot of $E(T',b)$ is shown in Fig. 7.

For a particular composite and given process variables, equation (8) can be used to calculate $\Delta t(T')$ as T' varies over the range $\left(1 \le T' \le T'_d\right)$. Figure 8 shows a plot of T' versus Δt for the baseline example of the Langley ATP robot applying PEEK/carbon composite tape, as

described in section 6. Note that T' is capped at T_d' to prevent degradation. Physically, this could be done by slightly defocusing the thermal input beam, as discussed in references 2 and 5. Since the lower end of the interval Δt can always be taken as zero, Fig. 8 is also a plot of T' versus t.

5. EFFECTIVE BONDING TIME

For a nonisothermal process, the effective bonding time t_{eff} relative to an isothermal process at T_g is given for a typical thermoplastic composite by (ref. 9)

$$t_{eff} = \int_0^{t_1} 10^{\frac{17.44\left[T(t)-T_g\right]}{516+T(t)-T_g}}\, dt \tag{9}$$

where the integrand is the universal WLF expression and the integration includes all periods for which $T(t) \geq T_g$. This equation is valid for temperatures $T(t)$ within about 100 K above T_g. However, for PEEK, T_d is 410 K above T_g, and an Arrhenius type of temperature dependence applies. Such a temperature dependence is included in an extended WLF expression, as given by Ferry (ref. 13)

$$t_{eff} = \int_0^{t_1} 10^{\frac{17.44(T-T_g)\left(1+\frac{259688}{T_g T}\left[.0249+.000482(T-T_g)\right]\right)}{516+T-T_g}}\, dt \tag{10}$$

If written in terms of the dimensionless temperature T', the extended WLF form for t_{eff} becomes

$$t_{eff} = \int_0^{t_1} 10^{\frac{17.44(T_g-T_\infty)(T'-1)\left(1+\frac{259688\left[.0249+.000482(T_g-T_\infty)(T'-1)\right]}{T_g\left[T_\infty+(T_g-T_\infty)T'\right]}\right)}{516+(T_g-T_\infty)(T'-1)}}\, dt \tag{11}$$

When integrated numerically for T' versus t, as plotted in Fig. 8 for the baseline example described in section 6, equation (11) gives $t_{eff} = 7.33\times10^{13}$ s. Finally, the mass and volumetric process rates are given by

$$\dot{M} = \rho U \tau w \tag{12}$$

and

$$\dot{V} = U \tau w \tag{13}$$

6. SENSITIVITY STUDIES

Baseline Example. Baseline process parameters, denoted by superscript 0, that approximate the present operating conditions of the Langley ATP robot are given by

$$w^0 = .0762 \quad \text{m}$$

$$\tau^0 = 1.27 \times 10^{-4} \quad \text{m}$$

$$U^0 = .085 \quad \text{m s}^{-1}$$

$$x_h{}^0 = 1.27 \times 10^{-3} \quad \text{m}$$

$$T_\infty{}^0 = 293.16 \quad \text{K} \tag{14}$$

Baseline material parameters for PEEK/carbon composite are given by (ref. 3)

$$\rho^0 = 1560 \quad \text{kg m}^{-1}$$

$$C_p{}^0 = 1425 \quad \text{J kg}^{-1}\,\text{K}^{-1}$$

$$K_{11}{}^0 = 6 \quad \text{W m}^{-1}\,\text{K}^{-1}$$

$$K_{22}{}^0 = .72 \quad \text{W m}^{-1}\,\text{K}^{-1}$$

$$T_g{}^0 = 413.16 \quad \text{K}$$

$$T_d{}^0 = 823.16 \quad \text{K} \tag{15}$$

For these baseline process and material parameters, the model yields the baseline results

$$b^0 = 20$$

$$Q_0{}^0 = 428.7 \quad \text{W}$$

$$t_{eff}{}^0 = 7.328 \times 10^{13} \quad \text{s}$$

$$\dot{M}^0 = 1.283 \times 10^{-3} \quad \text{kg s}^{-1}$$

$$\dot{V}^0 = 8.227 \times 10^{-7} \quad \text{m}^3\,\text{s}^{-1} \tag{16}$$

Sensitivity Studies. The computed results of individually varying the process parameters from their baseline values are summarized in Table 1.

Table 1. Process Sensitivity Study

	b / b^0	Q_0 / Q_0^0	t_{eff} / t_{eff}^0	$\dot{M} / \dot{M}^0$	$\dot{V} / \dot{V}^0$
$x_h / x_h^0 = 1.1$	1.1	1.05	1.20	1	1
$U / U^0 = .9$	.9	.95	1.12	.9	.9
$\tau / \tau^0 = .9$	1	1	1.11	.9	.9
$w / w^0 = .9$	1	.9	1	.9	.9
$T_\infty / T_\infty^0 = .9659$	1	1.08	1.25	1	1

The computed results of individually varying the material parameters from their baseline values are summarized in Table 2.

Table 2. Materials Sensitivity Study

	b / b^0	Q_0 / Q_0^0	t_{eff} / t_{eff}^0	$\dot{M} / \dot{M}^0$	$\dot{V} / \dot{V}^0$
$\rho / \rho^0 = .9$	.9	.95	1.01	.9	1
$C_p / C_p^0 = .9$	.9	.95	1.01	1	1
$K_{11} / K_{11}^0 = .9$	1.11	1	1.04	1	1
$K_{22} / K_{22}^0 = 1.1$	1	1.05	1.05	1	1
$T_g / T_g^0 = .9758$	1	.92	1.08	1	1
$T_d / T_d^0 = 1.024$	1	1	1.23	1	1

7. DISCUSSION

The sensitivity results for b / b_0, Q_0 / Q_0^0, $\dot{M} / \dot{M}^0$, and $\dot{V} / \dot{V}^0$ follow directly from (1c), (3a), (12), and (13). The results for t_{eff} / t_{eff}^0 are more complex, since they follow from (11), where T' as a function of t (or Δt) is given implicitly by (8), as illustrated for the baseline example by Fig. 8. Experience shows that the dominant contributions to t_{eff} come from the T' values that are close to T_d', where in the baseline example $T_d' = 4.167$.

Table 1. In Table 1, a 10 percent increase in x_h causes a 20 percent increase in t_{eff}, which is due to a 20 percent increase in $\Delta t(T_d')$. Fifteen percent of this increase comes from $x_h^{3/2}$ and 5 percent from an increase in efficiency $E(T_d', b)$ that results from the 10 percent increase in b. The 10 percent decrease in U causes a 12 percent increase in t_{eff} that is due to a 12 percent increase in $\Delta t(T_d')$. This increase results from a 17 percent increase due to $U^{-3/2}$ and a 5 percent decrease in $E(T_d', b)$ due to the 10 percent decrease in b. The 10 percent decease in thickness τ causes an 11 percent increase in t_{eff} due to τ^{-1} in (8a). The 10 percent decrease in tape width w leaves t_{eff} unchanged. A surprising result is that a 10 K decrease in tooling temperature T_∞ gives a 25 percent increase in t_{eff}. The explanation is that T_d' is decreased by 6 percent, which gives a 25 percent increase in $\Delta t(T_d')$ from a 20 percent increase in $(T_d')^{-3}$ and a 5 percent increase in $E(T_d', b)$.

Table 2. In Table 2, a 10 percent decrease in either ρ or C_p gives only a 1 percent increase in t_{eff} because the 5 percent increase in $\Delta t(T_d')$ due to $\rho^{-1/2}$ or $C_p^{-1/2}$ is counteracted by a 4 percent decrease in $E(T_d', b)$ due to the 10 percent decrease in b. The 10 percent decrease in longitudinal conductivity K_{11} gives a 4 percent increase in t_{eff} because the 11 percent increase in b gives a 4 percent increase in $E(T_d', b)$, which results in a 4 percent increase in $\Delta t(T_d')$. The 10 percent increase in K_{22} gives a 5 percent increase in t_{eff} simply because of the factor $K_{22}^{1/2}$ in $\Delta t(T_d')$.

Up to this point, the sensitivity studies may be viewed as stretching the time axis of the integral in (11). In the subsequent studies, the amplitude of the integrand will also be varied. A 10 K decrease in T_g gives an 8 percent increase in t_{eff}, as follows: This decrease in T_g results in an 9 percent increase in T_d', which causes a 32 percent decrease in $\Delta t(T_d')$ due to a 23 percent decrease in $(T_d')^{-3}$ and a 9 percent decrease in $E(T_d', b)$. However, this decrease in $\Delta t(T_d')$ is more than offset by a large increase in the integrand at $T' = T_d'$ to give t_{eff} a net increase of 8 percent. Finally, a 20 K increase in T_d results in a 23 percent increase in t_{eff}, as follows: This increase in T_d causes a 4 percent increase in T_d', which decreases $\Delta t(T_d')$ by 14 percent because of a 10 percent decrease in $(T_d')^{-3}$ and a 4 percent decrease in $E(T_d', b)$. However, this decrease in $\Delta t(T_d')$ is more than offset by a large increase in the integrand at $T' = T_d'$ to give t_{eff} a net increase of 23 percent.

The sensitivity studies show that t_{eff} can be substantially increased without decreasing the productivity rates $\dot{M}$ and $\dot{V}$ by increasing the consolidation length x_h, decreasing the tooling temperature T_∞, or increasing the degradation temperature T_d. Smaller increases in t_{eff} can be obtained without decreasing $\dot{M}$ and $\dot{V}$ by decreasing the longitudinal conductivity K_{11}, increasing the transverse conductivity K_{22}, or decreasing the glass transition temperature T_g. The thermal input power Q_0 can be reduced without decreasing $\dot{M}$ and $\dot{V}$ by decreasing the specific heat at constant pressure C_p or decreasing the glass transition temperature T_g. Decreasing the density ρ can also reduce Q_0 without reducing $\dot{V}$, although $\dot{M}$ will be reduced.

8. CONCLUSIONS

An earlier thermal model for *in-situ* automated tape placement (ATP) has been extended to lower values of the Peclet number. This extension brings the model to the present operating Peclet numbers of the Langley ATP robot. Sensitivity studies were performed about these operating conditions with PEEK/carbon composite. The model computes the effective bonding time referred to the glass transition temperature, the thermal input power, and the mass and volumetric process rates as functions of the process and material variables. The process variables are the consolidation length, the laydown speed, the width and thickness of the tape, and the temperature of the tooling. The material variables are the density, the specific heat at constant pressure, the longitudinal and transverse thermal conductivities, and the glass transition and degradation temperatures. The computed thermal input power always causes the temperature on the weld interface to decrease passively to the glass transition temperature at the downstream end of the consolidation head.

According to reptation theory, the interlaminar bond strength after wetting has occurred is proportional to the one-fourth power of the effective bonding time until full bonding is achieved. The sensitivity studies can be used as guides toward increasing the effective bonding time, decreasing the thermal input power, increasing the process rates, or otherwise optimizing the ATP process. A surprising result was that a 10 K decrease in the tooling temperature causes a 25 percent increase in the effective bonding time and an 8 percent increase in the thermal input power. The explanation is that reducing the tooling temperature also reduces the dimensionless degradation temperature, which increases the bonding efficiency. A 10 percent increase in the consolidation length was found to give a 20 percent increase in the effective bonding time and a 5 percent increase in the thermal input power. A 20 K increase in the polymer degradation temperature gives a 23 percent increase in the effective bonding time with no change in the thermal input power. Other smaller, but significant changes in effective bonding time, thermal input power, and process rates were obtained as each of the process and material parameters were individually varied.

REFERENCES

1. E. P. Beyeler and S. I. Güçeri, *Trans. ASME, 110*, 424-430 (1988).
2. S. M. Grove, *Composites, 19 (5)*, 367-375 (1988).
3. M. N. G. Nejhad, R. D. Cope, and S. I. Güçeri, *J. Thermoplastic Composite Materials, 4*, 20-45 (1991).
4. S. C. Mantell and G. S. Springer, *J. Composite Materials, 26 (16)*, 2348-2377 (1992).
5. R. G. Irwin, Jr. and S. I. Güçeri, *AMD-Vol. 194, Mechanics in Materials Processing and Manufacturing*, ASME, 319-333 (1994).
6. R. Pitchumani, R. C. Don, J. W. Gillespie, Jr., and S. Ranganathan in V. Prasad *et al*., eds., *HTD-Vol. 289, Thermal Processing of Materials: Thermal Mechanics, Controls and Composites,* ASME, 223-234 (1994).
7. J. A. Hinkley, R. W. Grenoble, and J. M. Marchello, *SAMPE International Symposium, 40*, 1560-1569 (1995).
8. A. Miller, C. Wei, and A. G. Gibson, *Composites Part A*, 27A, 49-56 (1996).
9. J. A. Hinkley, J. M. Marchello, and B. C. Messier, *SAMPE International Symposium, 41* (1996).
10. R. C. Costen and J. M. Marchello, *SAMPE International Symposium, 41*, 1346-1360 (1996).
11. R. E. Norris, *Mat. Tech.*, 9, 51-53 (1994).
12. R. C. Costen, NASA TN D-4244 (1967).
13. J. D. Ferry, *Viscoelastic Properties of Polymers*, Third Ed., Wiley, 287-290 (1980).

BIOGRAPHIES

Robert C. Costen is an applied mathematician at NASA-Langley who works in the Composites and Polymers Branch. He has authored and co-authored numerous modeling papers in materials processing, aerodynamics, atmospheric science, lasers, and radiation protection.

Joseph M. Marchello is a professor of civil and mechanical engineering at Old Dominion University. He is a chemical engineer with over 30 years of teaching and research experience in process development. He is author of over 100 technical and scientific papers.

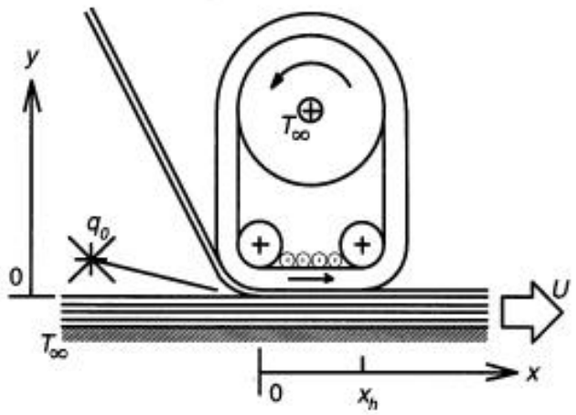

Figure 1. *In-situ* automated tape placement configuration.

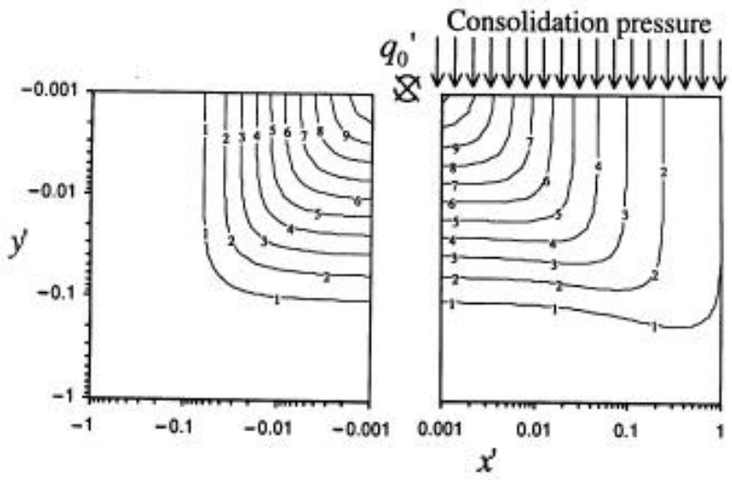

(a) $b = 10$

Figure 2. Dimensionless temperature $T'(x', y')$ isotherms in composite substrate for various values of $b = Pe / 2$.

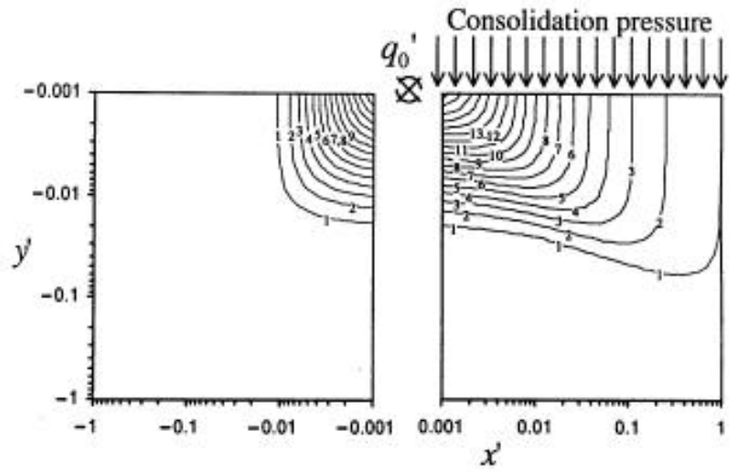

(b) $b = 100$

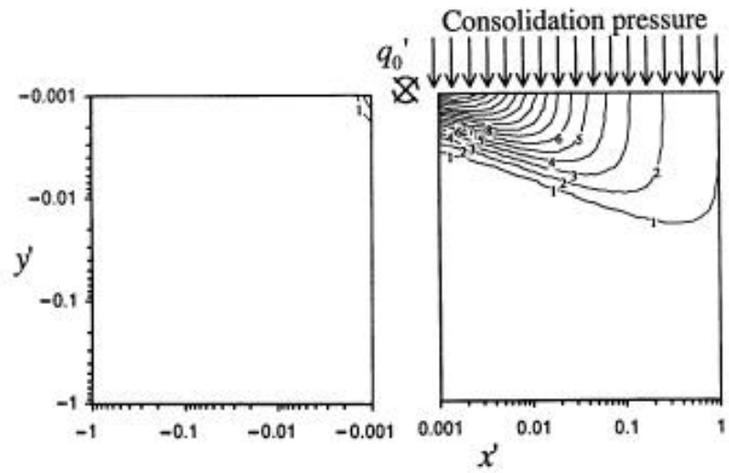

(c) $b = 1000$

Figure 2. Concluded.

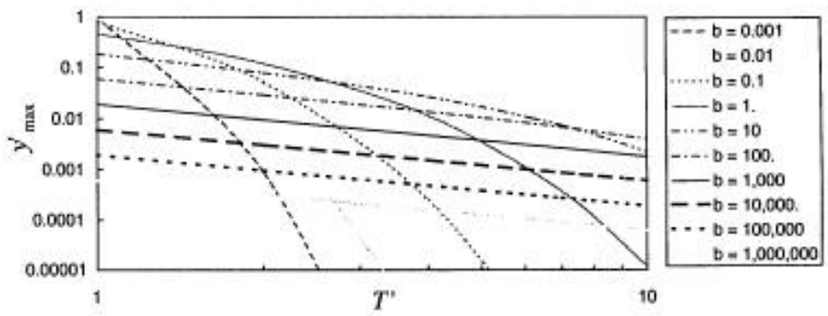

Figure 3. Dimensionless penetration depth y'_{max} of T'-isotherm versus T' for various b.

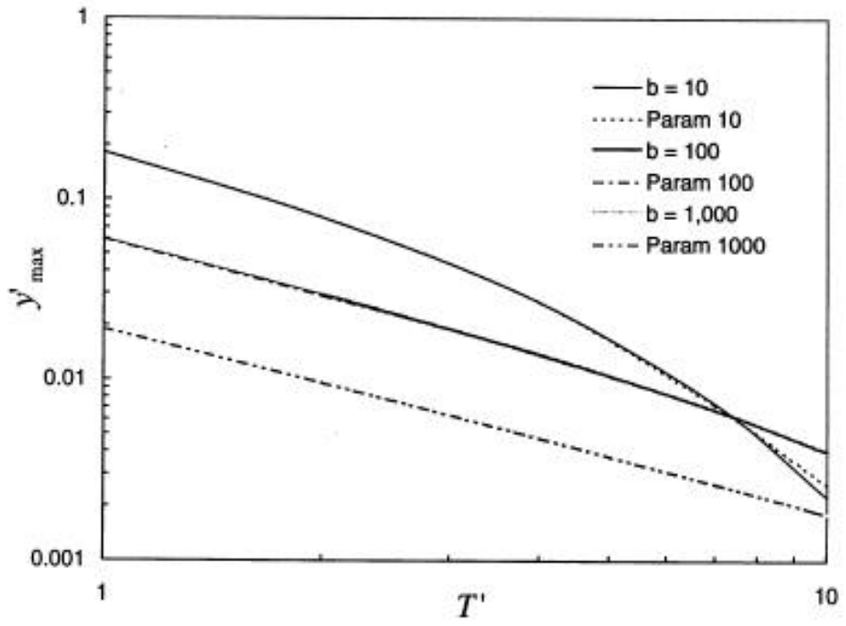

Figure 4. Comparison of exact and parameterized curves for y'_{max} versus T' for $b \geq 10$.

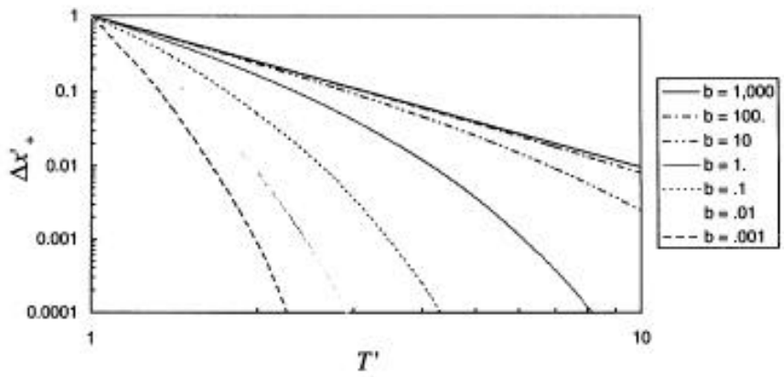

Figure 5. Positive segment $\Delta x'_+$ of x'-axis enclosed by T'-isotherm versus T' for various b.

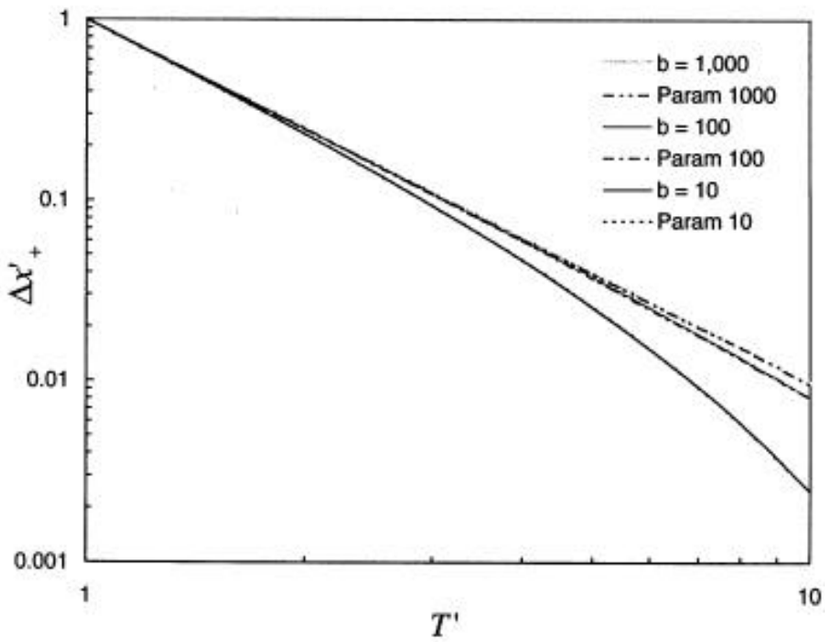

Figure 6. Comparison of exact and parameterized curves for $\Delta x'_+$ versus T' for $b \geq 10$.

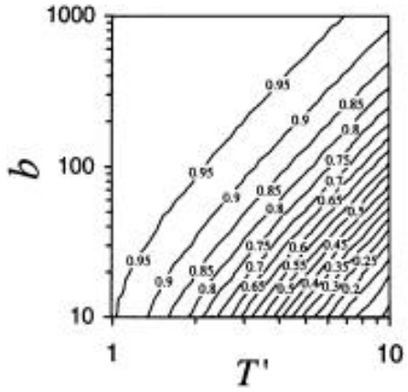

Figure 7. Contour plot of efficiency $E(T', b)$, as given by (8b).

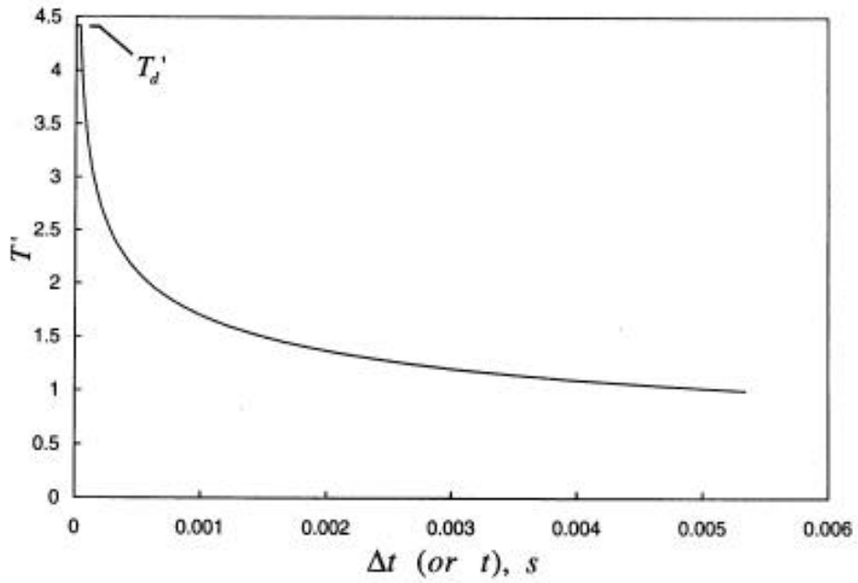

Figure 8. Dimensionless temperature T' versus accumulated time $\Delta t(T')$ that the dimensionless temperature of a material point on the weld interface equals or exceeds T', as given by (8). Abscissa Δt can be taken as t for numerical evaluation of integral in (11).